2007 IEEE International Conference on
Robotics and Automation
Roma, Italy, 10-14 April 2007

An Analytical Method for the Planning of Robust Assembly Tasks of Complex Shaped Planar Parts

A. Stemmer, A. Albu-Schäffer, G. Hirzinger
Institute of Robotics and Mechatronics, German Aerospace Center (DLR), Germany
E-mail: andreas.stemmer@dlr.de, alin.albu-schaeffer@dlr.de

Abstract— **The paper addresses the automatic assembly of planar parts with complex geometry. Its main focus is on the automatic generation and parameterization of the assembly sequence, which should provide maximal robustness with respect to positioning errors of the robot and residual position uncertainties of vision based object localization. The assembly utilizes active or passive compliance of the robot in order to align the parts automatically. Success of the automatic alignment, i.e. the convergence of the assembly process can be guaranteed using the means of regions of attraction (ROA). The planning optimizes the assembly trajectories and parameters in such a way that the ROA is maximized for a given part geometry. For the convergence analysis, passivity properties of the robot and the environment are used. The method is validated through extensive experiments and can be successfully applied also for the automated assembly planning with passive compliance devices, as widely used today in industrial automation.**

I. Motivation and Task Description

The target application aimed for the presented system is that of a robot assistant for humans working in industrial environments. The task of the robot is to execute assembly operations of parts with complex geometry (such as an automobile oil-pump or other objects of similar complexity) autonomously or in cooperation with humans. The present paper describes the assembly algorithms developed and tested on a set of planar objects with complex, non-convex geometric forms. The chosen task is a typical example of an industrial manufacturing process, which is still executed almost completely manually today, with a very low degree of automation. There are several aspects particular to this task which make the automation difficult. The requirement of high sensor capability, the complexity of the task programming, the limited velocity of force controlled industrial robots, the limited autonomy and flexibility are certainly some of them, leading to performance and success rates much below those of humans.

In order to be able to solve the proposed task with the required performance, vision and contact (force-torque) information are combined in the presented approach. Vision is used to determine a global (though not very precise) initial position estimation of the objects. The robot itself is limited in terms of absolute positioning accuracy with respect to a camera reference frame. Therefore, the main focus of the paper is on the development of an assembly strategy which uses the controlled compliance of the robot for achieving the required performance and robustness with respect to the mentioned positioning uncertainty. The idea is to shift the computationally intensive analysis of the part geometry and of the assembly motions to the planing phase, such that the resulting assembly process is maximally robust and can use simple and fast online control algorithms.

An important aspect for the simplification of the task programming is the automatic parameterization of the available controllers (e.g. parameterization of the stiffness of the impedance controller), as well as the automatic and robust assembly path generation for a given geometrical part. Robustness in this context requires a planning such that the convergence range, corresponding to the range of acceptable initial position estimation errors for robot and parts, is maximized. The final goal is to design a toolbox which, given the geometry of the parts (from CAD or from a vision system), can automatically generate the controller parameterization and the motion commands, e.g. directly in a robot programming language. This is the main new theoretical contribution of this paper, and is described in Sec. III. Experimental results on the assembly process using the proposed method are presented in Sec. IV.

II. Related Work

Although a lot of research has been done in the field of force and vision based robotic assembly, these advanced methods have never reached the state of robustness and simplicity which is needed for wide industrial or domestic applications. While force-motion control is one of the most classical and well established topics in robotics research [1], [2], [3], robots used for industrial assembly are normally not equipped with force/torque-sensors but use a passive compliance element. The so called *Remote Center Compliance* [4], [5] gives remarkable results for assembly tasks with small deviations, but it has to be adjusted for a given application and usually requires chamfers on the assembled parts. In some special applications, blind search algorithms can be used to extend the region of possible deviations [6], but for complex-shaped chamferless parts with small tolerances as described here, a blind search is too time-consuming for practical application.

Of course, more sophisticated solutions have been proposed in literature and validated experimentally. When talking about robotic assembly, most publications address strategies [7], [8] and optimizations [9] for the classic peg-in-hole problem. For geometrically simple parts, model-based strategies which observe the state of the assembly are feasible. By measuring forces and positions, the geometrical state of the objects is estimated continously [10], [11], [12] or at

least discrete contact states are distinguished [13], [14], [15]. Based on the estimations, appropriate corrective motions are executed. However, while the contact state graph of a peg-in-hole task is still clearly laid out, it explodes for complex shaped parts.

A slightly different approach uses the current force measurements directly for corrective motions [12], [16]. The difference is that no online model of the parts is needed in this case. This is the active version of the passive compliance with the same disadvantages concerning flexibility and reliability. In order to improve automated assembly and understand the problems better, some groups tried to analyze the human skills used for insertion tasks [17], [18].

The new approach proposed in this paper is different from the related ones in the sense that, instead of trying to exactly determine the location of parts and the contact state, it aims at reaching the maximal local robustness with respect to possible errors. This is achieved by means of geometrical and dynamical model based analysis and planning of the assembly trajectory. Although this idea is comparable to some work in the grasping community [19], [20], the application and the stability theory based approach differ significantly.

III. Robust Assembly Strategy

A. Basic Strategy

The basic idea of the presented assembly strategy is very similar to the way humans approach the problem. The geometry of the part and the rough information about the hole position is used to align the part automatically with the hole, just by pressing it against the contour of the hole and relying on the Cartesian compliance provided by the impedance controlled robot. The pressing allows the corners of the part to slide to the right position in a natural way, if the starting point and the target position of the impedance control are within certain limits. The allowable region of the starting point (as shown in Fig. 1) depends on the target position and the hole geometry and is called *region of attraction (ROA)* throughout this paper. It is the key element of the presented strategy and the remainder of this section will deal with the properties and selection of optimal ROAs for a given hole. It is obvious that the size of the ROA directly correlates with the robustness of the alignment process. The bigger the ROA is, the larger the allowed uncertainties are, since it is only necessary to position the part within the ROA. This way, the problem of robust assembly can be transformed into the problem of finding the largest ROA (and the according pushing direction and stiffness parameters) in the planning phase.

An example assembly sequence planned this way is shown in Fig. 2. The assembly starts with slightly tilting the part and then immersing a first corner into the hole. By pushing the part in the direction of the corresponding corner of the hole, the part will naturally slide to the right position and align itself. Prerequisite for success is that the initial position of the immersed corner lays within the ROA of the appropriate hole's corner and that the stiffness parameters are chosen properly. Assuming that the first corner is aligned properly,

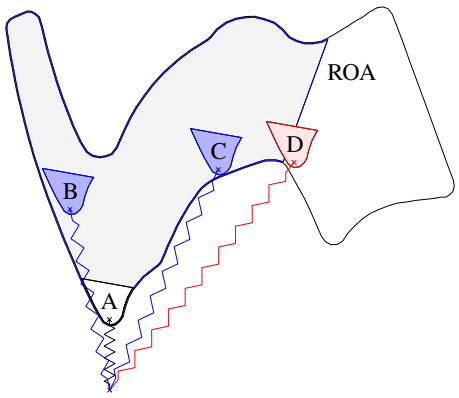

Fig. 1. A typical region of attraction (ROA) for an example part. The small part (representing the inserted corner) will be guided automatically to position A if the alignment process starts anywhere within the ROA (e.g. from B or C). If it starts outside (e.g. from D), it cannot be garantueed that the alignment will be successful.

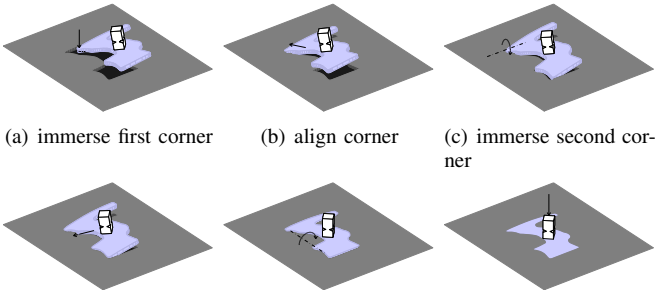

(a) immerse first corner (b) align corner (c) immerse second corner

(d) align whole part along edge (e) straighten up part (f) press in part

Fig. 2. Example of the presented strategy

a second contact point is needed to ensure the rotational alignment of the part. Having reached a stable two point contact, it is easy to straighten up the part and insert it completely.

B. Analytical Model

In order to better understand the alignment process during the assembly, a simplified model is considered and analysed (see Fig. 3). The following assumptions are made:

- The corner entering the hole is infinitesimally small, only translational movements are considered, therefore the part can be modelled as a single point.
- The relevant part of the hole's contour is given in form of the continuous and two times differentiable function $x_2 = c(x_1)$.
- The stiffness control of the robot is working ideally, providing a Cartesian spring behaviour which draws the mass point from the starting position $\boldsymbol{x} \in \mathbb{R}^2$ to the constant commanded position $\boldsymbol{x}_d \in \mathbb{R}^2$. The associated stiffness parameters are given by the positive definite matrices $\boldsymbol{K}_x = diag(k_i)$ for the spring constant and $\boldsymbol{D}_x = diag(d_i)$ for the damping coefficient.
- The compliance frame of the stiffness controller is selected in such a way that the x_2-axis is anti-parallel

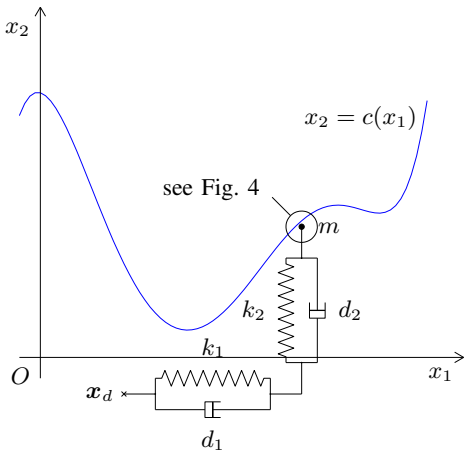

Fig. 3. Simplified model of the settling process. Only the spring-damper models of the impedance controlled robot are visualized, the additional force due to the contact with the environment is shown in Fig. 4

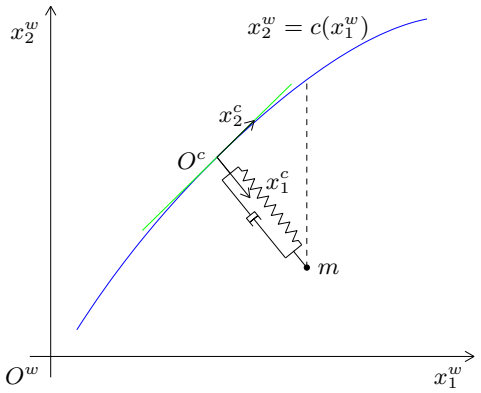

Fig. 4. Zoom of the situation in Fig. 3. The force due to the compliant contact model depends on the penetration depth.

to the desired pushing direction. Note that the resulting ROA and the final equilibrium point is influenced by the pushing direction. This gives another degree of freedom for the planner.

For the analysis we are considering the robot equations written in Cartesian coordinates. The gravity term is already compensated by low level torque control. The dynamical behaviour of the system can be described as an ordinary second order differential equation

$$\boldsymbol{M}_x(\boldsymbol{q})\ddot{\boldsymbol{x}} + \boldsymbol{\mu}_x(\boldsymbol{q},\dot{\boldsymbol{q}})\dot{\boldsymbol{x}} = \boldsymbol{F}_i(\boldsymbol{x},\dot{\boldsymbol{x}}) + \boldsymbol{F}_c(\boldsymbol{x},\dot{\boldsymbol{x}}) \quad (1)$$

In order to avoid unnecessary complexity of the derivation, the Cartesian mass matrix $\boldsymbol{M}_x(\boldsymbol{q})$ is assumed to have dimension 2×2, the extension to the 6DOF case is obvious. Accordingly, $\boldsymbol{\mu}_x(\boldsymbol{q},\dot{\boldsymbol{q}})$ which contains the Coriolis and centrifugal terms, is of dimension 2. The vector $\boldsymbol{q} \in \mathbb{R}^m$ contains the m joint positions. $\boldsymbol{F}_i$ is the control input. We are assuming a simple Cartesian compliance controller of the form

$$\boldsymbol{F}_i(\boldsymbol{x},\dot{\boldsymbol{x}}) = -\boldsymbol{K}_x(\boldsymbol{x} - \boldsymbol{x}_d) - \boldsymbol{D}_x\dot{\boldsymbol{x}} \quad (2)$$

such that the motion of the system is described by

$$\boldsymbol{M}_x(\boldsymbol{q})\ddot{\boldsymbol{x}} + \boldsymbol{\mu}_x(\boldsymbol{q},\dot{\boldsymbol{q}})\dot{\boldsymbol{x}} + \boldsymbol{D}_x\dot{\boldsymbol{x}} + \boldsymbol{K}_x(\boldsymbol{x} - \boldsymbol{x}_d) = \boldsymbol{F}_c(\boldsymbol{x},\dot{\boldsymbol{x}}). \quad (3)$$

$\boldsymbol{F}_c$ represents the force emerging from contact with the environment, i.e. the contour of the hole. For the modelling of the contact forces, the common Hunt-Crossley model [21], [22] is used, which relates the contact forces to a non-linear spring-damper system representing the environment. It is usually given in its one dimensional form

$$F = -\lambda\delta^n\dot{\delta} - k_e\delta^n, \quad (4)$$

where λ, n and k_e are positve scalar constants depending on the geometry and materials involved, δ is the penetration depth. By using this model, discontinuities of the forces at the contact are avoided. The system is Lipschitz continuous, making it possible to apply standard Lyapunov analysis. In order to use the Hunt-Crossley model in this scenario and apply it to our two-dimensional problem, a transformation of coordinates as indicated in Fig. 4 is introduced. The coordinate system denoted by superscript $()^c$ is attached to the given contour of the hole and moving with the sliding part. It is chosen in such a way that contact forces are only acting in x_1^c-direction which is always normal to the curve. Correspondingly, the x_2^c-direction is tangential to the curve. Assuming a stiff environment, the penetration depth remains small and the direction of x_2^c can be approximated by the tangent of the curve at point $[x_1^w, c(x_1^w)]^T$. The superscript $()^w$ emphasizes the reference to the world coordinate system to avoid confusion, but all coordinates without superscript are referred to the world coordinate system as well, $\boldsymbol{x} \equiv \boldsymbol{x}^w$. The local (curvilinear) coordinates $\boldsymbol{x}^c$ are related to $\boldsymbol{x}^w$ through the relation $\boldsymbol{x}^c = \boldsymbol{h}(\boldsymbol{x}^w)$, which can be derived from simple geometric considerations:

$$\boldsymbol{x}^c = \begin{bmatrix} \sqrt{\frac{1}{1+c'^2}}(c - x_2^w) \\ \int_0^{x_1^w} (1 + c'^2)\, d\tilde{x}_1^w \end{bmatrix} \quad (5)$$

where c is an abbreviation for $c(x_1^w)$, $c' = \frac{\mathrm{d}c(x_1^w)}{\mathrm{d}x_1^w}$ and $c'' = \frac{\mathrm{d}^2 c(x_1^w)}{(\mathrm{d}x_1^w)^2}$. The Jacobian of this transformation is given by

$$\begin{aligned} \boldsymbol{J}(\boldsymbol{x}^w) &= \left[\frac{\partial \boldsymbol{h}_i(\boldsymbol{x}^w)}{\partial \boldsymbol{x}_j^w}\right] \\ &= \begin{bmatrix} \sqrt{\frac{1}{1+c'^2}}\left(\frac{c'c''(x_2-c)}{1+c'^2} + c'\right) & -\sqrt{\frac{1}{1+c'^2}} \\ 1 + c'^2 & 0 \end{bmatrix} \end{aligned} \quad (6)$$

Its transpose $\boldsymbol{J}^T$ maps the contact force into the reference coordinate system

$$\boldsymbol{F}_c^w = \boldsymbol{J}^T\boldsymbol{F}_c^c. \quad (7)$$

The penetration depth $\delta \geq 0$ of the Hunt-Crossley model is related to the curve coordinate system by

$$\delta = \begin{cases} x_1^c = h_1(\boldsymbol{x}^w), & x_1^c \geq 0 \\ 0, & x_1^c < 0. \end{cases} \quad (8)$$

Please note that due to the non-linear properties of the Hunt-Crossley model, the force is always continuous. Combining (3), (4) and (7), we finally get the differential equation

for our system:

$$\boldsymbol{M}_x(\boldsymbol{q})\ddot{\boldsymbol{x}} + \boldsymbol{\mu}_x(\boldsymbol{q},\dot{\boldsymbol{q}})\dot{\boldsymbol{x}} + \boldsymbol{D}_x\dot{\boldsymbol{x}} + \boldsymbol{K}_x(\boldsymbol{x}-\boldsymbol{x}_d) + \boldsymbol{J}(\boldsymbol{x})^T \begin{bmatrix} \lambda\delta^n\dot{\delta} + k_e\delta^n \\ 0 \end{bmatrix} = \boldsymbol{0} \tag{9}$$

For easier reading, we keep the notation of δ as an abbreviation for the penetration depth $\delta = x_1^c = h_1(\boldsymbol{x}^w)$.

Equilibrium points $\boldsymbol{x}^*$ of the system satisfy the condition

$$\boldsymbol{K}_x(\boldsymbol{x}^* - \boldsymbol{x}_d) + \boldsymbol{J}(\boldsymbol{x}^*)^T \begin{bmatrix} k_e(\delta^*)^n \\ 0 \end{bmatrix} = \boldsymbol{0}, \tag{10}$$

which leads to the unique solution

$$\boldsymbol{x}^* = \boldsymbol{x}_d \tag{11}$$

for the trivial case $x_{d,2} > c(x_{d,1})$, i.e. $\boldsymbol{x}_d$ is located in free space and no contact occurs. For the contact case, an approximation of the solutions $\boldsymbol{x}^*$ of (10) is possible. Assuming that the stiffness k_e of the environment is much larger than any element of the programmed stiffness $\boldsymbol{K}_x$ of the robot, one can conclude that $\delta \to 0^+$, since $\boldsymbol{J} \neq \boldsymbol{0}$. This means that the equilibrium points will be on the contour $x_2 = c(x_1)$ and therefore $x_2^* - c \approx 0$ can be assumed in the Jacobian (6). By eliminating $k_e(\delta^*)^n$ from (10), one obtains the scalar equation

$$k_1(x_1^* - x_{d,1}) + k_2(c(x_1^*) - x_{d,2})c'(x_1^*) = 0. \tag{12}$$

Obviously, the equilibrium points depend on the selected stiffness parameters $k_{1,2}$ and the target position $\boldsymbol{x}_d$, as well as on the gradient of the curve c'. The next section will prove local asymptotic stability for these equilibrium points. Afterwards, important properties for the local robustness of the equilibria will be discussed.

C. Stability and Convergence

Using the method of Lyapunov and the Invariance Principle of LaSalle, it is possible to show the stability and convergence of the system, if the starting point is within a certain ROA, depending on the selected equilibrium point $\boldsymbol{x}^*$. Consider the Lyapunov function candidate

$$V(\boldsymbol{x},\dot{\boldsymbol{x}}) = \tfrac{1}{2}\dot{\boldsymbol{x}}^T\boldsymbol{M}_x(\boldsymbol{q})\dot{\boldsymbol{x}} + \tfrac{1}{2}(\boldsymbol{x}-\boldsymbol{x}_d)^T\boldsymbol{K}_x(\boldsymbol{x}-\boldsymbol{x}_d) + \frac{1}{n+1}k_e\delta^{n+1} - V_0, \tag{13}$$

$$V_0 = \tfrac{1}{2}(\boldsymbol{x}^*-\boldsymbol{x}_d)^T\boldsymbol{K}_x(\boldsymbol{x}^*-\boldsymbol{x}_d) + \tfrac{1}{n+1}k_e(\delta^*)^{n+1}. \tag{14}$$

Using the symmetry properties of $\boldsymbol{M}_x$ and $\boldsymbol{K}_x$ and the skew symmetry of $\frac{1}{2}\dot{\boldsymbol{M}}_x - \boldsymbol{\mu}_x(\boldsymbol{q},\dot{\boldsymbol{q}})$, it is easy to show that

$$\dot{V}(\boldsymbol{x},\dot{\boldsymbol{x}}) = -\dot{\boldsymbol{x}}^T\boldsymbol{D}_x\dot{\boldsymbol{x}} - \lambda\delta^n\dot{\delta}^2 \leq 0. \tag{15}$$

Furthermore, $V(\boldsymbol{x}^*+\Delta\boldsymbol{x}, \boldsymbol{0}+\dot{\Delta\boldsymbol{x}}) - V(\boldsymbol{x}^*,\boldsymbol{0})$ can be shown to be positive definite in a vicinity of $\boldsymbol{x}^*$ for all $\Delta\boldsymbol{x} > \boldsymbol{0}$ as long as $c''(\boldsymbol{x}^*) \geq 0$.

Given a simply connected, open subset $\boldsymbol{E} \subset \mathbb{R}^4$ around one selected equilibrium point $[\boldsymbol{x}^{*T}, \dot{\boldsymbol{x}}^T = \boldsymbol{0}]^T$, defined by

$$V(\boldsymbol{x},\dot{\boldsymbol{x}}) < V_b \quad \forall \quad [\boldsymbol{x}^{*T},\dot{\boldsymbol{x}}^T]^T \in \boldsymbol{E} \tag{16}$$

$$V(\boldsymbol{x},\dot{\boldsymbol{x}}) = V_b \quad \forall \quad [\boldsymbol{x}^{*T},\dot{\boldsymbol{x}}^T]^T \in \partial\boldsymbol{E}. \tag{17}$$

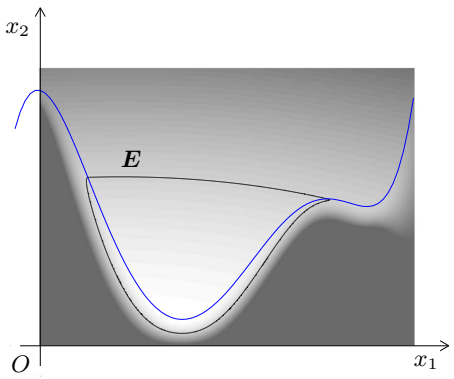

Fig. 5. Potential $V(\boldsymbol{x})$ for the example shown in Fig. 3 with $\dot{\boldsymbol{x}} = \boldsymbol{0}$, $k_1 = 1$, $k_2 = 5$ and a relatively low environment stiffness of $k_e = 10^3$. Darker color indicates higher energy. The black equipotential is the border of the ROA E.

V_b is chosen as big as possible, such that $[\boldsymbol{x}^{*T}, \dot{\boldsymbol{x}}^T = \boldsymbol{0}]^T$ is the only equilibrium point fulfilling $\dot{V} = 0$ within $\boldsymbol{E}$ (see Fig. 5). We can then see, that

$$V(\boldsymbol{x},\dot{\boldsymbol{x}}) \geq 0 \quad \forall \quad [\boldsymbol{x}^{*T},\dot{\boldsymbol{x}}^T]^T \in \boldsymbol{E} \tag{18}$$

$$V(\boldsymbol{x},\dot{\boldsymbol{x}}) = 0 \quad \Leftrightarrow \quad \boldsymbol{x} = \boldsymbol{x}^*, \dot{\boldsymbol{x}} = \boldsymbol{0} \tag{19}$$

$$\dot{V}(\boldsymbol{x},\dot{\boldsymbol{x}}) \leq 0 \quad \forall \quad [\boldsymbol{x}^{*T},\dot{\boldsymbol{x}}^T]^T \in \mathbb{R}^4, \tag{20}$$

hence the system is locally asymptotically stable and converges to $\boldsymbol{x}^*$ if the starting point is contained in the ROA $\boldsymbol{E}$. The reader will have noticed that the ROA is now applied to the whole state space of the system, including the initial velocities, whereas the originial definition in Sec. III-A only included the initial position. This enhancement can be helpful for the planning of highly dynamical assembly tasks where the initial velocities are not zero. However, in most practical cases, the assembly starts from a steady state and the initial velocities may be neglected.

D. Robustness

Given the analysis of the previous section, the robustness of the assembly process can be maximized by choosing the parameters appropriately. Because usually the position information about the hole is afflicted with uncertainty (i.e. the exact position of the coordinate system relative to the robot base is not known), the commanded desired position relative to the contour of the hole will be afflicted with uncertainty as well. Therefore the goal of the insertion planning is to have the equilibrium point be maximally insensitive against variations of the desired position. A variation of the desired position

$$\boldsymbol{x}_d \longrightarrow \boldsymbol{x}_d + \Delta\boldsymbol{x}_d \tag{21}$$

due to uncertainties leads to an unwanted variation of the equilibrium point

$$\boldsymbol{x}^* \longrightarrow \boldsymbol{x}^* + \Delta\boldsymbol{x}^*. \tag{22}$$

Considering only small deviations, the sensitivity of the system can be expressed based on the approximation made

in (12) as

$$\left.\frac{\Delta x_1^*}{\Delta x_{d,1}}\right|_{\Delta x_{d,2}=0} \approx \frac{k_1}{k_1 + k_2 c'^2 + k_2 c''(c - x_{d,2})} \stackrel{!}{=} 0 \quad (23)$$

$$\left.\frac{\Delta x_1^*}{\Delta x_{d,2}}\right|_{\Delta x_{d,1}=0} \approx \frac{k_2 c'}{k_1 + k_2 c'^2 + k_2 c''(c - x_{d,2})} \stackrel{!}{=} 0 \quad (24)$$

Without further calculations, it can be seen that for optimal robustness, the equilibrium point should be chosen to have large curvature $c''(x_1^*)$, which is a very intuitive requirement. For low curvatures the consideration of friction effects is crucial, which will be subject of future research on this topic. The stiffness parameter k_1 should be chosen as low as possible, but in practice a lower boundary is given due to unwanted friction effects. k_2 should be as big as necessary to generate an appropriate normal force. Of course k_2 is limited by the maximum force allowed for the given part and by the expected variations of the position estimation.

As only small deviations are considered here, the analysis of this section provides information about the local robustness of the assembly only. In order to have maximum global robustness, these findings have to be combined with the global properties of the ROA as described in the previous section.

E. Implementation

Based on the analysis shown above, a simplified protoypic implementation has been programmed in Matlab. The algorithm analyzes the geometrical properties of the given part and extracts possible ROAs for various pushing directions. Assuming that the conditions for robustness as calculated above (k_1 very low compared to k_2) are fulfilled and that the initial velocities are zero, the determination of the ROAs can be reduced to a simple geometric partitioning of the hole's surface. Fig. 6 shows the partitioning and the resulting ROAs and destination corners for some particular pushing directions. To use the ROAs for the insertion of the type of

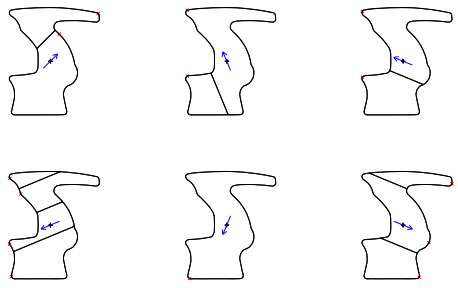

Fig. 6. ROAs for different pushing directions

parts described above, further analysis of the geometry of the part is necessary. The main goal is to find the corners of the hole which have the maximum ROA. The first step of the analysis is therefore the search for possible candidate corners. This is done by sampling all possible pushing directions with a step size depending on the complexity of the part and doing the geometric partitioning for those directions as shown in Fig. 6. Corners that have a ROA which is bigger than the expected uncertainty are possible candidates for contact points and further evaluation is necessary. Only corners which are on the part's convex hull have to be considered, because only those are usable for immersion into the hole. Based on the found *single* contact candidates, *pairs* of contact points have to be built, since two contact points are needed for the rotational alignment of the part. The pairs are then rated by reachability and symmetry of levers.

This first part of the geometrical analysis is purely based on the hole's geometry, the ROAs determined here are valid for infinitesimal small object vertices only. Having a real corner of the part immerse into the hole, the corresponding ROAs become significantly smaller, even more when considering some degree of initial rotational misalignment of part and hole. Therefore the selected contact point candidates are now validated with a real 3D model of the tilted part entering the hole. The algorithm uses basically a Minkowski sum of the hole's contour and the pentrating cross-section of the part's corner. Details about the shrinking of the ROAs through transfer in the 3D domain can be found in [23].

The leftover contact point candidates can now be rated by size of ROA and lever ratio. The contact point pair with the highest rating provides the best possible robustness for the given part and is therefore selected for the assembly. Having the desired contact points, it is not difficult to automatically generate code for the robot's programming language which executes the motions as shown in Fig. 2. Execution times for a complete analysis of a part like the one shown in Fig. 6 are in the range of several minutes, therefore online path planning is not yet possible. However, the current implementation is only a prototypic proof-of-concept programmed in Matlab and no speed optimization has been pursued so far.

IV. Experimental Results

The evaluation of the robustness of the presented strategy was performed on the setup shown in Fig. 7. The DLR industrial robot assistant uses a manipulator based on the DLR light-weight robot technology. The robot has a very light-weight structure compared to its workload and an inherent joint elasticity, thus limiting the internal energy and forces of the system and improving the reaction time during contact. It is equipped with torque sensors in each joint as well as with a force-torque sensor at the wrist. The first offer the possibility of fast local control at joint level, leading to response times which can hardly been achieved using a wrist sensor only; the latter could be used (but was not in this experiment) for fine additional sensing of the tip interaction forces. Since the robot can sense the interaction along the entire structure, it can also be used by a human as an input device for teaching parts of the application.

The impedance controller used for the DLR light-weight robot is more complex than the controller considered in Sec. III. It takes into consideration the effects of joint flexibility and accesses the local joint torque controllers. However, the entire control structure is developed within a passivity framework and therefore, seen from its Cartesian

Fig. 7. Experimental setup for the assembly task using the DLR lightweight robot.

interface, the controlled robot is a passive system [24]. Thus a very similar (though requiring considerably more involved computations) Lyapunov analysis to the one in Sec. III can be done, just by using the appropriate energy function for the controlled robot together with the contact potential energy.

The experimental task consists in the insertion of three planar acryllic glass parts with a clearance of less than $0,1\text{mm}$ into corresponding holes. The plate with the appropriate holes was fixed on the table for the experiments described in next section and was freely movable when using an additional vision system (Sec. IV-B).

A. Statistical Evaluation of Robustness

In order to evaluate the robustness of the presented strategy, numerous assemblies of the three example parts were accomplished. The hole position was known exactly (within the accuracy of the robot) in this case and an artificial uncertainty was added randomly in the range from 0 to 20mm of lateral offset in any direction and in the range of $\pm 5°$ of rotational error. The results for the three considered example parts and the optimal insertion strategy are given in Fig. 8 and in Table I. For the part "PAPAS", two different strategies (the first one as delivered by the algorithm, the second one chosen manually as the next best intuitive guess) are compared. The marked areas within the figures represent the amount of uncertainty which we required to be handled by the algorithm. The uncertainties given by a simple vision system have for example this order of magnitude. The method provided 100% success rate within this area.

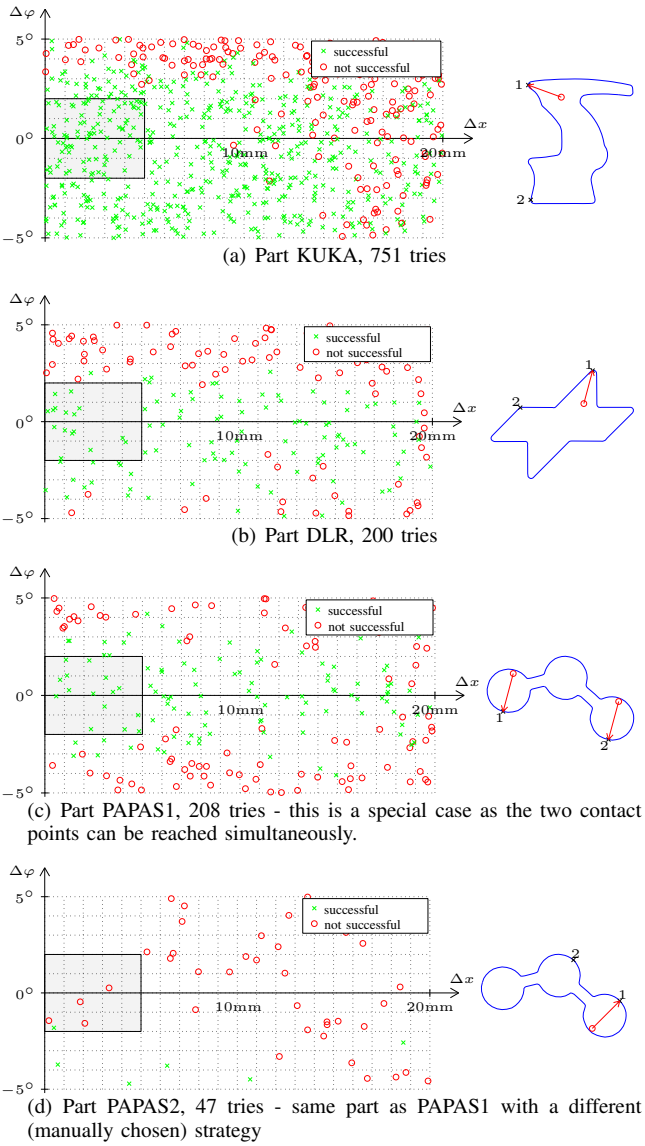

(a) Part KUKA, 751 tries

(b) Part DLR, 200 tries

(c) Part PAPAS1, 208 tries - this is a special case as the two contact points can be reached simultaneously.

(d) Part PAPAS2, 47 tries - same part as PAPAS1 with a different (manually chosen) strategy

Fig. 8. The experimental results of the compliance based assembly for the considered range of position estimation errors. Each mark represents one insertion try, the region of expected position uncertainty is marked. On the right side, the chosen strategy for the specific part (selected contact points, pushing direction) is visualized.

B. Insertion Experiments in Combination with Vision

On the *Automatica 2006* fair in Munich, we demonstrated the automatic assembly using the presented robust planning algorithm. The setup was extended by a vision system consisting of a single PAL color camera for the localization of the holes on the table. The image processing is based on standard hardware components and uses color segmentation and affine invariant feature classification. A more detailed overview of the vision system and the setup can be found in [25].

The uncertainties of the vision system were in the range of 1mm translational and $1°$ rotational error. As expected, the summed errors of the image based position estimation and of the robot Cartesian positioning accuracy are too high

TABLE I
EXPERIMENTAL RESULTS: RATE OF SUCCESSFUL INSERTIONS

part	whole range $(0-20\mathrm{mm}, \pm 5^\circ)$		region of interest $(0-5\mathrm{mm}, \pm 2^\circ)$	
KUKA	558/751	74,3%	88/88	100%
DLR	112/200	56,0%	16/16	100%
PAPAS1	114/208	54,8%	15/15	100%
PAPAS2	6/47	12,8%	1/5	20%

for a successful direct insertion of the parts (which have a tolerance of about $0.1\mathrm{mm}$). Using the presented strategy however, the task can be successfully accomplished, since the overall positioning accuracy is considerably higher than requested by the compliance based insertion algorithm. The setup reached a high success rate throughout the four days of the fair and confirmed the promising preliminary results. The accompanying video clip shows such an experiment in which the plate is arbitrarily placed on the table, then the plate and the holes are localized by the vision system and finally the parts are successfully inserted using the presented robust assembly strategy.

V. CONCLUSIONS

The experiments demonstrated that an offline assembly planning strategy combined with robust compliant execution can be used to enhance the flexibility and speed of an assembly process. For complex geometric parts, high robustness with respect to position uncertainty (stemming from the vision system and the robot) can be achieved by maximizing the ROA through an appropriate planning of the trajectory and the stiffness. By using a controller which allows the representation of the system as an interconnection of passive subsystems (including the contacted environment) a local convergence analysis can be done under some simplifying assumptions (e.g. exact friction compensation). This analysis leads also for the real system to increased performance, as illustrated by the experiments.

REFERENCES

[1] N. Hogan, "Impedance control: An approach to manipulation, part I - theory, part II - implementation, part III - applications," *Journ. of Dyn. Systems, Measurement and Control*, vol. 107, pp. 1–24, 1985.

[2] O. Khatib, "A unified approach for motion and force control of robot manipulators: The operational space formulation," *RA*, vol. RA-3, pp. 43–53, 1987.

[3] B. Siciliano and L. Villani, *Robot Force Control*. Kluwer Academic Publishers, Boston, MA, 1999.

[4] D. E. Whitney and J. L. Nevins, "What is the remote center compliance and what can it do?" in *9th International Symposium on Industrial Robots*, Washington, D. C., 1978.

[5] H. Asada and Y. Kakumoto, "The dynamic RCC hand for high speed assembly," in *Proceedings of the 1988 IEEE International Conference on Robotics and Automation*, Philadelphia, USA, April 1988, pp. 120–125.

[6] W. S. Newman, M. S. Branicky, H. A. Podguski, S. Chhatpar, L. Huang, J. Swaminathan, and H. Zhang, "Force-responsive robotic assembly of transmission components," in *Proceedings of the 1999 IEEE International Conference on Robotics and Automation*, Detroit, Michigan, May 1999, pp. 2096–2102.

[7] T. Lozano-Pérez, M. T. Mason, and R. H. Taylor, "Automatic synthesis of fine-motion strategies for robots," *The International Journal of Robotics Research*, vol. 3, no. 1, pp. 3–24, 1984.

[8] H. Bruyninckx, S. Dutré, and J. D. Schutter, "Peg-on-hole: a model based solution to peg and hole alignment," in *Proceedings of the 1995 IEEE International Conference on Robotics and Automation*, Nagoya, Japan, May 1995, pp. 1919–1924.

[9] N. Yamanobe, Y. Maeda, T. Arai, T. Kato, T. Sato, and K. Hatanaka, "Design of damping control parameters for peg-in-hole by industrial manipulators considering cycle time," in *Proceedings of the 2004 IEEE/RSJ International Conference on Intelligent Robots and Systems*, Sendai, Japan, September 2004, pp. 3351–3356.

[10] J. D. Schutter, H. Bruyninckx, S. Dutré, J. D. Geeter, J. Katupitiya, and S. Demey, "Estimating first order geometric parameters and monitoring contact transitions during force controlled compliant motion," in *Int. Jounrnal of Robotic Research*, vol. 18, 1999, pp. 1161–1184.

[11] G. E. Hovland and B. J. McCarragher, "Combining force and position measurements for the monitoring of robotic assembly," in *Proceedings of the 1997 IEEE/RSJ International Conference on Intelligent Robots and Systems*, Grenoble, France, September 1997.

[12] W. S. Newman, Y. Zhao, and Y.-H. Pao, "Interpretation of force and moment signals for compliant peg-in-hole assembly," in *Proceedings of the 2001 IEEE International Conference on Robotics and Automation*, Seoul, Korea, May 2001, pp. 571–576.

[13] U. Thomas, B. Finkemeyer, T. Kröger, and F. M. Wahl, "Error-tolerant execution of complex robot tasks based on skill primitives," in *Proceedings of the 2003 IEEE International Conference on Robotics and Automation*, Taipei, Taiwan, September 2003, pp. 3069–3075.

[14] J. Xiao, "Goal-contact relaxation graphs for contact-based fine motion planning," in *IEEE International Symposium on Assembly and Task Planning*, Marina del Rey, California, August 1997, pp. 25–30.

[15] G. Milighetti, H.-B. Kuntze, C. W. Frey, B. Distel-Feddersen, and J-Balzer, "On a primitive skill-based supervisory robot control architecture," in *Proceedings of the 4th German Conference on Robotics ROBOTIK*, Munich, Germany, May 2006.

[16] S. C. Kang, Y. K. Hwang, M. S. Kim, C. W. Lee, and K.-I. Lee, "A compliant motion control for insertion of complex shaped objects," in *Proceedings of the 1997 IEEE International Conference on Robotics and Automation*, Albuquerque, New Mexico, April 1997, pp. 841–846.

[17] P. Sikka and B. J. McCarragher, "Rule-based contact monitoring using examples obtained by task demonstration," in *International Joint Conferences on Artificial Intelligence*, 1997, pp. 514–521.

[18] Y. Yamamoto and T. Hashimoto, "Task analysis of ultra-precision assembly processes for automation of human skills," in *Proceedings of the 2001 IEEE/RSJ International Conference on Intelligent Robots and Systems*, Maui, Hawaii, October 2001, pp. 2093–209.

[19] M. T. Mason, "Manipulator grasping and pushing operations," Ph.D. dissertation, MIT, 1982.

[20] K. Gopalakrishnan and K. Goldberg, "Gripping parts at concave vertices," in *Proceedings of the 2002 IEEE International Conference on Robotics and Automation*, Washington, DC, May 2002, pp. 1590–1596.

[21] K. H. Hunt and F. R. E. Crossley, "Coefficient of restitution interpreted as damping in vibroimpact," in *Transactions of the ASME Journal of Applied Mechanics*, 1974, pp. 440–445.

[22] D. W. Marhefka and D. E. Orin, "A compliant contact model with nonlinear damping for simulation of robotic systems," in *IEEE Transactions on Systems, Man and Cybernetics*, vol. 29, November 1999, pp. 566–572.

[23] A. Stemmer, "Entwurf und Implementierung robuster Fügestrategien für impedanzgeregelte Roboter," Master's thesis, Technische Universität München, 2005.

[24] A. Albu-Schäffer, C. Ott, and G. Hirzinger, "Passivity based cartesian impedance control for flexible joint manipulators," *Proc. 6-th IFAC-Symposium on Nonlinear Control Systems, Stuttgart*, vol. 2, p. 111, 2004.

[25] A. Stemmer, G. Schreiber, K. Arbter, and A. Albu-Schäffer, "Robust assembly of complex shaped planar parts using vision and force," in *Proceedings of the International Conference on Multisensor Fusion and Integration for Intelligent Systems*, 2006, pp. 493–500.